

Investigation of ammonium diuranate calcination with high-temperature X-ray diffraction

R. Eloirdi · D. Ho Mer Lin · K. Mayer ·
R. Caciuffo · T. Fanghänel

Received: 12 May 2014 / Accepted: 16 August 2014 / Published online: 9 September 2014
© The Author(s) 2014. This article is published with open access at Springerlink.com

Abstract The thermal decomposition of ammonium diuranate (ADU) in air is investigated using in situ high-temperature X-ray diffraction (HT-XRD), thermogravimetry and differential thermal analysis. Data have been collected in the temperature range from 30 to 1000 °C, allowing the observation of phase transformation and the assessment of the energy changes involved in the calcination of ADU. The starting material $2\text{UO}_3 \cdot \text{NH}_3 \cdot 3\text{H}_2\text{O}$ undergoes a process involving several endothermic and exothermic reactions. In situ HT-XRD shows that amorphous UO_3 is obtained after achieving complete dehydration at 300 °C, and denitration at about 450 °C. After cooling from heat treatment at 600 °C, a crystalline UO_3 phase appears, as displayed by ex situ XRD. The self-reduction of UO_3 into orthorhombic U_3O_8 takes place at about 600 °C, but a long heat treatment or higher temperature is required to stabilise the structure of U_3O_8 at room temperature. U_3O_8 remains stable in air up to 850 °C. Above this temperature, oxygen losses lead to the

formation of U_3O_{8-x} , as demonstrated by subtle changes in the diffraction pattern and by a mass loss recorded by TGA.

Introduction

Ammonium diuranate $(\text{NH}_4)_2\text{U}_2\text{O}_7$ (ADU), once used to create coloured glazes in ceramics, is the most prominent chemical compound among the uranium ore concentrates, often referred to as “yellow cake”: ADU plays also an important role in the fabrication of uranium oxide fuel. For this reason, ADU is of great interest for nuclear forensics, a relatively young discipline that aims at providing hints on the history and intended use of nuclear materials of unknown origin, on the basis of certain measurable parameters that, as fingerprints, are characteristics of the material, of the place where it was produced and of the route followed for its transformation [1–6].

The term “ammonium diuranate” is actually a misnomer, but it remains of common use. Controversies over the composition and structure of ADU have sparked numerous studies [7–13]. Its morphology has also attracted a great deal of attention, as it is well established that the characteristics of precursor materials are inherited into the final product [14, 15]. Laboratory-scale preparations of ADU are usually based on the reaction of UO_3 or uranyl nitrate with water and ammonia [8, 16], or by the reaction between hydrated UO_3 with liquid or gaseous ammonia [11, 16]. On the other hand, industrial productions are based on two routes, either via uranyl nitrate with aqueous or gaseous ammonia, or via the reaction of uranyl fluoride with ammonium hydroxide [15]. Industrial processes often include drying the wet concentrate at 120–400 °C or calcinations at 400–850 °C, resulting in the possibility of mixtures. Since the properties of the final product depend

R. Eloirdi (✉) · D. Ho Mer Lin · K. Mayer · R. Caciuffo ·
T. Fanghänel

European Commission, Joint Research Centre, Institute for
Transuranium Elements, P.O. Box 2340, 76125 Karlsruhe,
Germany

e-mail: rachel.eloirdi@ec.europa.eu

D. Ho Mer Lin

e-mail: Doris.HO-MER-LIN@ec.europa.eu

K. Mayer

e-mail: Klaus.MAYER@ec.europa.eu

R. Caciuffo

e-mail: Roberto.CACIUFFO@ec.europa.eu

T. Fanghänel

e-mail: Thomas.FANGHAENEL@ec.europa.eu

on the starting material, it is important to understand the decomposition steps and the intermediate products of the ammonium diuranate. Some studies have been previously reported, however the method of preparation and used techniques were different. For instance, in the report by Price and Stuart [17], nitrate-free ADU was prepared, and the thermal decomposition was monitored by TG with accompanying infrared spectroscopy data. As mentioned by Woolfrey [16], the thermal decomposition of ammonium uranates studied by some authors was not in complete agreement. In more recent publications, scanning electron microscopy and ex situ XRD were used to study calcined ADU, but only for a few selected temperatures [18], deduced from to exothermic and endothermic peaks observed by TG/DTA analyses and characteristic of the intermediate products of the reaction.

In this study, we have applied high-temperature X-ray diffraction (HT-XRD), thermogravimetry and differential temperature analyses (TG/DTA) as complementary tools for retracing and understanding the process leading to the decomposition of ADU under air. The investigated temperature spanned the range between 30 and 1000 °C. Although the XRD analysis does not permit an accurate determination of oxygen positions in heavy metal oxides, it enables one to follow the changes in the crystallographic structure, which can be correlated with the variation of mass detected by TG and the energy transfer measured by DTA. To the best of our knowledge, no studies of ADU decomposition based on in situ HT-XRD have been reported so far. The results obtained are compared with those gathered by ex situ XRD, focussing on the different phases appearing along the heat treatment. Finally, we discuss the formation of U_3O_8 above 600 °C and its stability with temperature, an interesting issue due to the use of U_3O_8 as a preferred storage form [19]. Also, the main purpose of this paper is to see the potential of HT-XRD associated to TG/DTA as a tool for nuclear forensic investigations.

Experimental

Synthesis of ADU

Ammonium hydroxide (Merck, 25 % w/v solution) was added manually in drop-wise fashion to 100 g/L of uranyl nitrate hexahydrate (purity 99 %) ($UO_2(NO_3)_2 \cdot 6H_2O$) which was constantly stirred (~ 250 rpm) at 68 °C [20]. The initial pH of uranyl nitrate solution was about 2, and the final pH after the completion of NH_4OH addition was about 11. The yellow precipitate was subsequently filtered and washed three times with ultrapure water (18 M Ω) and was allowed to dry overnight at room temperature. A few grams of material were obtained.

Instrument

TG/DTA analyses were carried out under flow of oxygen (4 N) at a heating rate of 10 °C/min on a temperature range of 30 °C till 1000 °C. The apparatus used was NETZSCH Simultaneous Analyzer STA 449 Jupiter. In situ HT-XRD patterns were acquired with a Bruker D8 powder diffractometer installed in a glove-box and mounted in a Bragg–Brentano configuration with a curved Ge monochromator (111), a Cu X-ray tube (40 kV, 40 mA), a Vantec detector and an Anton Paar HTK2000 heating chamber equipped with a Pt heating plate. Data were collected over a full diffraction angle range $2\theta = 10^\circ$ – 100° , in steps of 0.017° , with a counting time per step of 2 s. The explored temperature range spanned the interval 30–1000 °C, with the sample kept under static synthetic air (21 vol% O_2 + 79 vol% N_2) with a starting pressure of 800×10^2 Pa. Prior to measurement, MgO was used to check the calibration of the furnace chamber. Temperature errors were determined to fall within 5 % in the whole investigated interval. Ex situ XRD patterns were acquired with a Bruker D8 diffractometer similar to the in situ HT-XRD apparatus but using a Lynxeye detector and a Si wafer (111) as a sample holder.

Results

X-ray diffraction patterns of starting and final material

The XRD pattern of the starting material measured at 30 °C is shown in Fig. 1a. All diffraction peaks can be matched to those reported in the ICDD database (PDF number 00-044-0069) for the hexagonal structure of $2UO_3 \cdot NH_3 \cdot 3H_2O$. The precipitation of the ADU obtained by adding a large excess of ammonia, leads to a well-defined composition [11]. The oxidation state +VI of the reference material is in agreement with the yellow colour of the ADU sample (inset of Fig. 1a).

Figure 1b illustrates the room temperature XRD pattern of an ADU sample after heat treatment in air up to 1000 °C during the in situ HT-XRD investigation. This pattern can be fitted with the orthorhombic structure of U_3O_8 (Space Group C2 mm, No. 38), PDF number 01-074-2101 [21].

Thermogravimetry and differential thermal analyses of ADU

The TG/DTA curves of the ADU sample are reported in Fig. 2. For a better description, the data is denoted in five parts (I–V) that correspond largely to the appearance of endothermic and exothermic peaks.

The shoulder and the peak, noted as I and II, respectively, occur at about 100 and 200 °C and correspond to the

Fig. 1 **a** X-ray diffraction pattern of ADU sample (starting material) matched to reference material ($2\text{UO}_3\cdot\text{NH}_3\cdot 3\text{H}_2\text{O}$) shown in red -PDF (00-044-0069) The inset shows a picture of the sample; the yellow colour is characteristic of the ADU material. **b** X-ray diffraction pattern of an ADU sample obtained after a heat treatment up to $1000\text{ }^\circ\text{C}$ in air, matched to that of the reference material (U_3O_8) shown in blue colour (PDF 01-074-2101) The dark colour of the sample (inset) is characteristic of U_3O_8 (Color figure online)

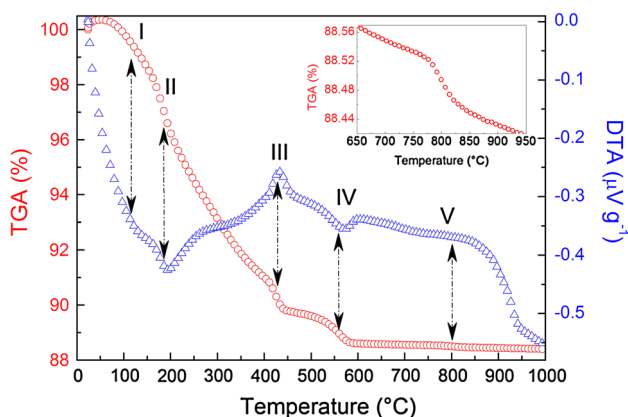
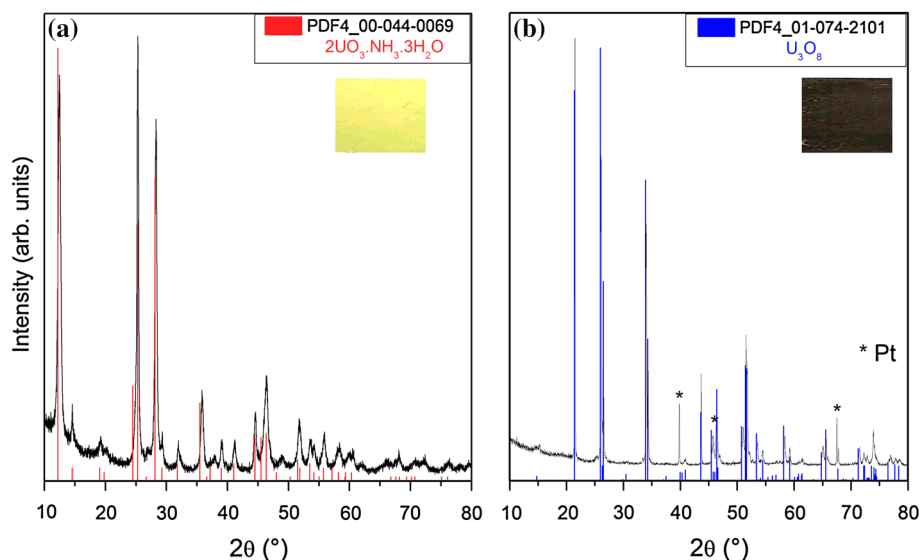


Fig. 2 Thermogravimetry curve (circles) and differential thermal curve (triangles) of the ADU sample. Inset details of the DTA curve in the range $650\text{--}950\text{ }^\circ\text{C}$

removal of physically and chemically adsorbed water molecules. Because of the superposition of the peaks, the TG curve analysis can be at best semi-quantitative. Thus, for the starting material sample whose XRD pattern is assigned to $2\text{UO}_3\cdot\text{NH}_3\cdot x\text{H}_2\text{O}$, TG/DTA reveals a mass loss of 7 wt% of water, taking place at about $300\text{ }^\circ\text{C}$. This gives rise to 2.5 mol number of water in the sample which is quite close to the data reported in literature [9]. The difference could be explained by the temperature considered for complete dehydration. Considering that the denitration begins at $300\text{ }^\circ\text{C}$ and completes at about $450\text{ }^\circ\text{C}$, the mass loss of NH_3 of about 3 wt% corresponds to 0.5 mol of NH_3 for 1 mol of UO_3 . From literature [16], we know that ammonia is strongly bound and that below $250\text{ }^\circ\text{C}$, and it is not taken out from the uranates. However, the dehydration and denitration of the sample cannot be fully differentiated on a temperature range of $250\text{--}400\text{ }^\circ\text{C}$ and, for this reason,

the quantification of the nitrate and water losses can only be approximated.

The exothermic peak (III) occurring at about $420\text{ }^\circ\text{C}$ can be related to the denitration of the sample. After denitration and formation of UO_3 , a constant mass is maintained over $100\text{ }^\circ\text{C}$ before reduction to U_3O_8 . Such behaviour has been reported in a study of UO_3 with amorphous structure [22]. This is followed by an endothermic peak (IV) occurring slightly above $550\text{ }^\circ\text{C}$ which corresponds to the self-reduction of UO_3 into U_3O_8 [17]. This will be further described by the HT-XRD study. The crystallisation of UO_3 coincides with a mass loss of about 1.5 wt%, and is assigned to its reduction into U_3O_8 as seen later by HT-XRD. However, this mass loss leads to a stoichiometry of $\text{UO}_{2.73}$ instead of $\text{UO}_{2.67}$ expected for U_3O_8 . In fact, the exact stoichiometry of U_3O_8 is difficult to obtain. Indeed, the O/U ratio deviates significantly from $8/3$ depending on the heating, temperature, time and thermal history [23]. Also the oxygen content cannot be precisely determined with the used TG/DTA device or X-ray diffraction. However, at about $800\text{ }^\circ\text{C}$ (peak V), a further weight loss takes place without any correlation in the DTA curve (inset Fig. 2). This could be related to the transition from U_3O_8 to U_3O_{8-x} , a structural change that does not affect significantly the energy of the system.

Above $850\text{ }^\circ\text{C}$, a drastic drop in the DTA curve occurs, which may correspond to the decomposition of the sample without mass loss, as demonstrated by the constant TG curve in this high temperature range. Above $900\text{ }^\circ\text{C}$, there is a decrease in the DTA curve, representative of an endothermic process completed at a temperature higher than $1000\text{ }^\circ\text{C}$. A similar DTA peak was reported earlier in literature [24] and was attributed to the conversion of U_3O_{8-x} to U_8O_{21} [25].

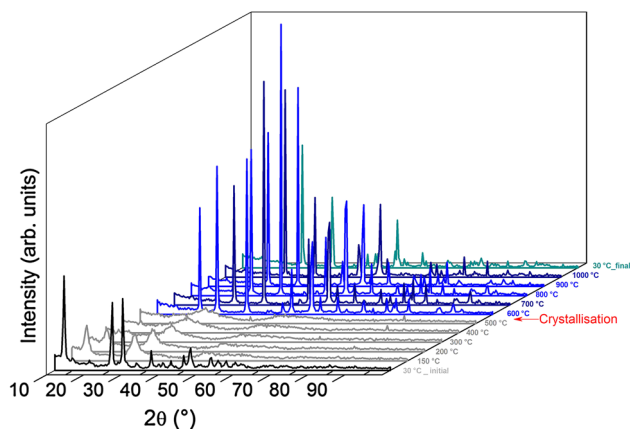


Fig. 3 In situ HT-XRD study of the decomposition of ADU in air, measured from 30 to 1000 °C, in addition to the normal XRD pattern measured after cooling to 30 °C

High-temperature X-ray diffraction of ADU

In order to study the decomposition of ADU and to understand the evolution of its structure with temperature, diffraction patterns have been measured with the sample kept at various temperatures up to 1000 °C. The results are shown in Fig. 3. A qualitative analysis of the diffraction profiles immediately reveals a transformation from a partially crystalline structure at room temperature to an amorphous state between 150 and 500 °C, until eventually a highly crystalline phase abruptly appears at 600 °C. As described in “[Thermogravimetry and Differential Thermal Analyses of ADU](#)” Section, ADU is reactive at a temperature range of 100–600 °C, where a handful of endothermic and exothermic peaks appear in the TG/DTA curve. This is in contrast with HT-XRD which shows mainly the appearance of weak and broad intensity peaks relating to the presence of disorder in the material. When combined, Figs. 2 and 3 provide complementary information on the process of ADU decomposition in air.

In the following, the different XRD patterns observed with in situ HT-XRD are compared to those observed with ex situ XRD made after isothermal treatment in TG/DTA. In Fig. 4, XRD patterns obtained from both instruments are placed side by side. As an example, pattern (a) is the profile measured in situ with HT-XRD at 150 °C, whereas the pattern (a′) is measured at room temperature on the sample that had been heated at 150 °C in air. At this temperature, we do expect the loss of physically absorbed water molecules, which still induces disorder in the material as seen by the broader peaks in HT-XRD. The cooling leads to a better-defined pattern very close to the one of the starting material (Fig. 1a). The decrease in the intensity of few peaks could be due to the loss of the physically absorbed

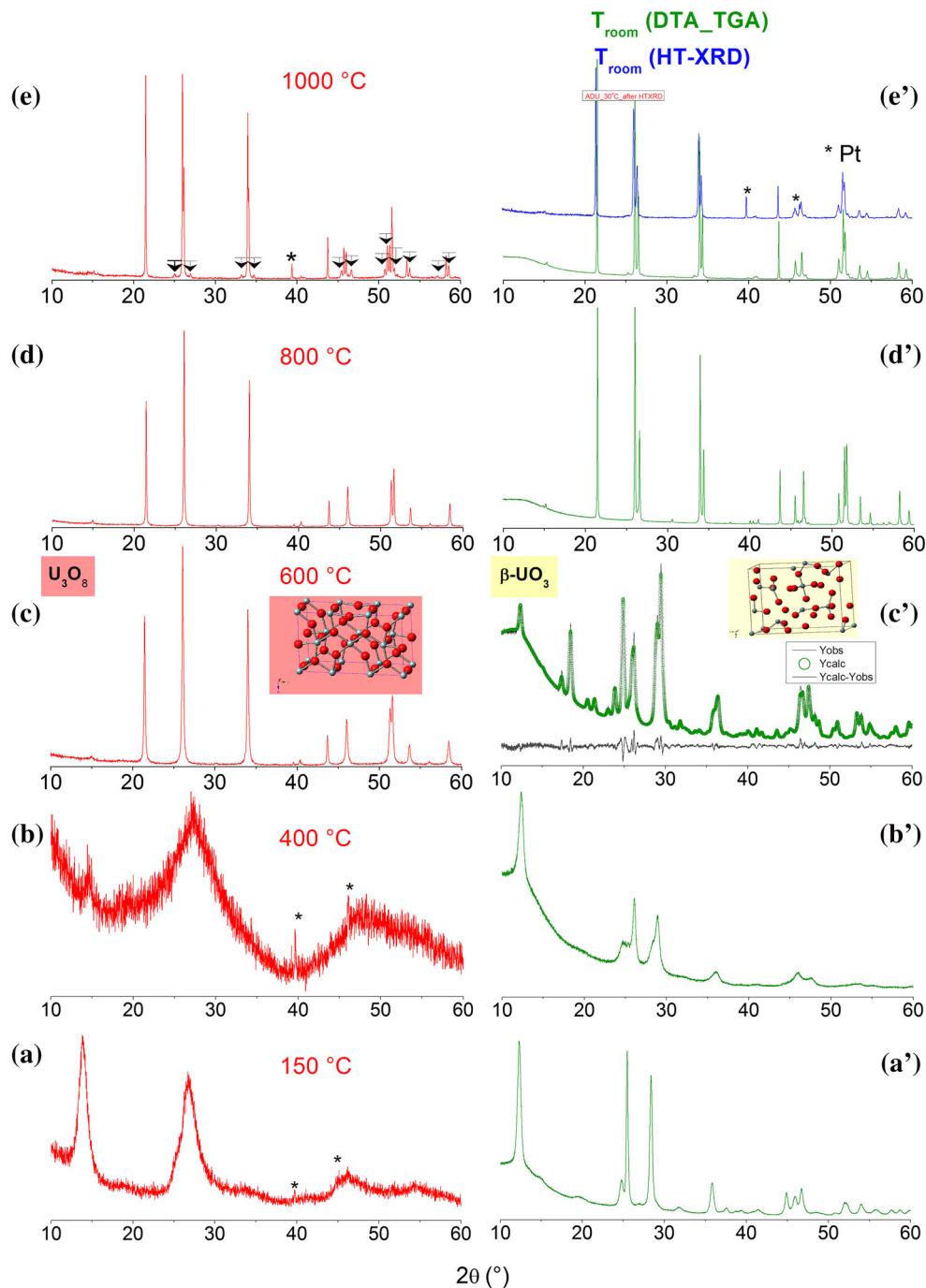
water. It has been reported that dehydration of minerals occurs in several steps and each accompanied by structural changes and a decrease in interlamellar spacing [17].

The HT-XRD pattern (b) measured at 400 °C displays even broader peaks than at a lower temperature, thus indicating a rather amorphous material. After cooling, such sample (pattern b′) still shows similarities with the sample cooled from 150 °C (pattern a′), with a further decrease in intensity and linewidth of the peaks. Based on the information given by the TG/DTA at this temperature, the loss of chemically absorbed water is completed, while the process of denitration is still on-going. The HT-XRD pattern obtained at 500 °C (Fig. 3) is similar to the one reported for 400 °C (pattern b). Thus, after complete denitration, expected for the sample measured at 500 °C, the resulting UO_3 is amorphous as reported in the literature for one of its known structures [19, 22]. Indeed, it has been reported in literature that UO_3 has one amorphous and six crystalline modifications (α , β , δ , ϵ , γ , ζ) [23].

At 600 °C (pattern c), the sudden crystallisation of the sample is revealed by the appearance of sharp peaks. These peaks could be easily assigned to U_3O_8 with an orthorhombic structure (Space Group $C2/m$, No. 38). The result is in agreement with the one reported in Ref. [26], where the structure of U_3O_8 was determined by a combination of HT-XRD and neutron diffraction. The in situ HT-XRD sample measured at 600, 700 and 800 °C (pattern d) are similar. The sample measured at 600 °C is metastable. The diffraction profile recorded for this sample after cooling down to room temperature is shown in panel (c′) of Fig. 4. The refinement of the diffraction pattern corresponds to β - UO_3 with a monoclinic structure (Space Group $P12_1/11$, No. 4), see inset of Fig. 4. Thus, during cooling from 600 °C, U_3O_8 (panel c) absorbs oxygen and gives rise to crystalline β - UO_3 (panel c′). This result is in agreement with literature reporting that for the formation of U_3O_8 from UO_3 , a heat treatment at 650 °C for 1 h is necessary, whereas at 600 °C, the process would be extremely slow [19]. The structure of U_3O_8 appeared stable at 800 °C as observed in both patterns (d) and (d′). The only difference induced by temperature is related to the lattice expansion. Thus, at this temperature, the loss of water and nitrate is complete, U_3O_8 is stoichiometric and is the main phase even after heat treatment at 1000 °C (patterns e and e′).

However, at 1000 °C (pattern e), extra peaks appear (indicated by arrows) that are not observed at 800 °C. This could be assigned to a symmetry lower than orthorhombic or to the formation of a multiphase mixture. Therefore, the orthorhombic U_3O_8 structure is stable up to 800 °C. However, the cooling of the sample in air shows the recovery of the stable structure and the presence of one single phase. Oxygen lost upon heating U_3O_8 above 800 °C

Fig. 4 *Left* In situ HT-XRD of an ADU sample measured at 150, 400, 600, 800 and 1000 °C. *Right* Ex situ XRD of ADU samples measured at room temperature after heat treatment at 150, 400, 600, 800 and 1000 °C

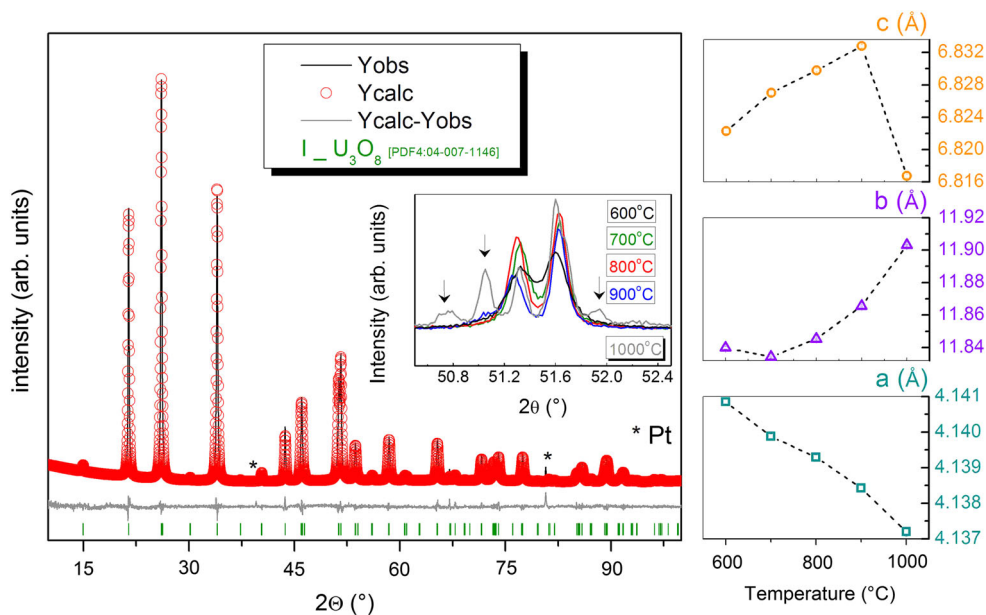


is rapidly replaced upon cooling [27]. In order to demonstrate that ex situ XRD measurements made at room temperature can be correlated to in situ HT-XRD, the XRD patterns recorded at room temperature on the sample obtained after heat treatment of 1000 °C in in situ HT-XRD and in ex situ with TG/DTA were compared. Both patterns are completely identical, indicating that the processes taking place through ex situ heat treatment can be correlated to the in situ process.

Le Bail refinement of HT-XRD pattern of ADU from 600 to 1000 °C

In this section, we focus on the HT-XRD pattern obtained at 600 °C (Fig. 5), corresponding to U_3O_8 with an orthorhombic structure (Space Group $C2/m$, No. 38). In the inset of Fig. 5, three patterns were compared on a limited 2θ range (50.4° – 52.6°). The pattern obtained at 600 °C is completely similar to those obtained at 700 and 800 °C.

Fig. 5 Le Bail refinement of HT-XRD pattern of ADU sample heated at 600 °C. *Inset* Effect of heat treatment on ADU at 600, 700, 800, 900 and 1000, as shown on a 2θ range (50.4°–52.6°). *Right* Lattice parameters evolution from 600 to 1000 °C in air



The main effect of the temperature is the shift of the peaks, due to the lattice expansion. However, peaks obtained at 600 °C are broader than those obtained at higher temperature, showing that the structure is less ordered and less stable, as demonstrated by the change of the pattern when the cooling of the sample is taking place (Fig. 4c'). At 900 °C, the pattern is also in a first glance similar to those obtained at 600 °C, however a small extra peak appears, as shown in the inset at about 51° in 2θ . This demonstrates that the sample structure of U_3O_8 at this temperature is unstable in air. This structural change is emphasised in the heat treatment done at 1000 °C, where additional and higher intensity peaks appear (indicated by arrows in the inset of Fig. 5). This change clearly shows that the optimal temperature for obtaining U_3O_8 is around 700 °C and that its stability in air decreases at higher temperatures.

The evolution of the lattice parameters of U_3O_8 as a function of temperature is reported on the right hand side of Fig. 5. We still consider the same structure for the pattern obtained at 1000 °C in order to refine the lattice parameters for comparisons with the patterns obtained at 600 °C. The lattice expansion takes place mainly along the b and c axes, whereas along a, the lattice expansion is weakly negative. The trend along the lattice c is broken for the sample treated at 1000 °C, thus emphasising the instability and/or the change of the U_3O_8 structure at this temperature. This result is in agreement with literature indicating that heating U_3O_8 during 1 h in oxidising atmosphere at 750 °C will achieve thermal stabilisation [19]. The thermal expansion of U_3O_8 is anisotropic as reported by Ackermann et al. [21].

Discussion

Figure 6 illustrates the evolution of the position of the Bragg diffraction peaks observed by HT-XRD together with the derivative curve $dTGA/dT$ versus the temperature. To discuss the different steps taking place during the calcination of ammonium diuranate, the mechanism is summarised in Table 1.

Below 600 °C, very few and broad peaks can be observed by HT-XRD, due to the disorder in the material. Indeed, the ADU sample obtained by precipitation still contains water and nitrate molecules giving rise to a weak crystallinity. Thus, in this range of temperature, XRD is not a very suitable characterisation tool.

Following the evolution of the $dTGA/dT$ curve, the mass loss can be correlated with water molecules (peak I and II) and nitrate (peak III). The crystallisation of the material observed at about 600 °C by HT-XRD is preceded by a mass loss appearing at 550 °C (peak IV) which can be explained by the self-reduction and phase transition of amorphous material UO_3 to highly crystalline material U_3O_8 . Until the formation of crystalline UO_3 and U_3O_8 , X-ray diffraction does not provide any information about the decomposition products.

The formation of U_3O_8 is stable in air in the temperature range of 700–800 °C. Above this range, a mass loss takes place, as shown by peak V in TG/DTA curve, very likely related to oxygen loss. Also, this is emphasised by in situ HT-XRD by a change of structure, as demonstrated by extra peaks from 900 °C on. Slow formation of another phase has been reported in literature [23] in α - U_3O_8 which can take

Fig. 6 Thermal decomposition of ADU sample in air. *Top* HT-XRD peaks position versus temperature with 2θ angle (10° – 80°). *Bottom* dTGA/dT curve

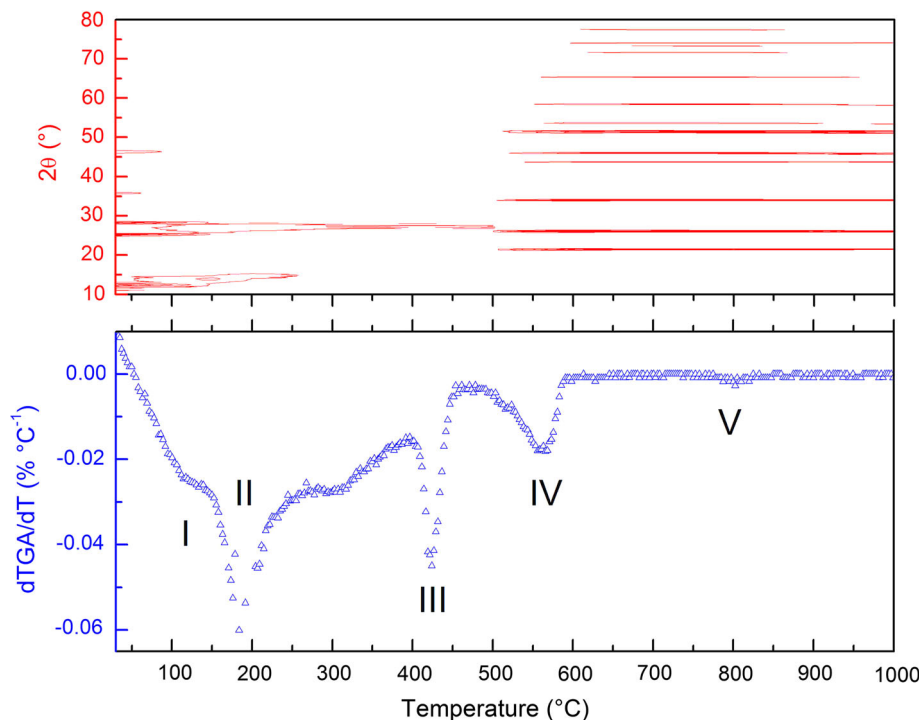


Table 1 Mechanisms of the process taking place in the calcination of ADU

Step	I	II	III	IV	V
Reaction	$2\text{UO}_3 \cdot \text{NH}_3 \cdot x\text{H}_2\text{O}$ $2\text{UO}_3 \cdot \text{NH}_3 \cdot x\text{OH}$	$2\text{UO}_3 \cdot \text{NH}_3 \cdot x\text{OH}$ $2\text{UO}_3 \cdot \text{NH}_3$	$2\text{UO}_3 \cdot \text{NHO}_3$ 2UO_3	3UO_3 U_3O_8	U_3O_8 U_3O_{8-x}

The table gives the first row the different steps, noted I till V, of the ADU calcination process based on the endothermic and exothermic peaks of the DTA and dTGA/dT curves reported in Figs. 1 and 6 respectively. The second row report the possible reaction for each step

place at the temperature range of 1000 – 1300 °C. This has been linked to a possible U_8O_{21} phase with a homogeneity range extending between the compositions $\text{UO}_{2.60}$ and $\text{UO}_{2.65}$ [23]. A slightly different composition range, $\text{UO}_{2.617}$ – $\text{UO}_{2.655}$ has also been reported [28]. It is possible that the proper stoichiometry of β - U_3O_8 is U_8O_{21} , since β - U_3O_8 has been prepared by heating α - U_3O_8 to 1350 °C followed by slow cooling to room temperature [29]. However it has often been reported that in this region, the phase is considered hypostoichiometric (U_3O_{8-x}) [23]. Two modifications of U_3O_8 , α and β - U_3O_8 crystallise both in orthorhombic system and their crystal structures are very similar. These compounds have a layer structure related to the hypostoichiometric “ideal” UO_3 structure which has uranyl bonds perpendicular to the layer. The difficulty to

rearrange the oxygen atoms in these infinite layer structures is probably the reason [23] for the slow equilibration between U_3O_8 and the gas phase at different temperatures and the oxygen partial pressures. The O/U ratio of the “ U_3O_8 ” phase varies with the experimental method used to determine it. Above 727 °C, the upper phase boundary was observed to have $O/U = 2.667$ (stoichiometry of U_3O_8) up to 1127 °C. At an ambient pressure of 0.21 atm O_2 , the compound however becomes hypostoichiometric above 600 °C [23].

The present study shows the potential use of HT-XRD together with TG/DTA as a potential tool for nuclear forensic investigations. Main results obtained in this study are in agreement with those reported in literature. The present material was prepared in our laboratory and

analysed to collect the so-called ‘fingerprints’ in a database. This latter can then be used for comparison to identify any material relevant to nuclear security. For the future, different compositions of yellow cake can be prepared and analysed in the same way as the present study. This will provide hints on the processing history of any material found in the framework of nuclear forensics investigations. Based on the TG/DTA analyses, characteristic temperatures can be chosen and used to retrace the corresponding initiated product through the in situ analyses of HT-XRD. In this study, we did report for the first time, in situ HT-XRD analyses of ADU decomposition. This confirms the crystallisation of the material after 500 °C and the stability of U_3O_8 under air in a temperature range between 700 and 800 °C. The transition of $\beta-UO_3$ to U_3O_8 could also be observed and confirmed only by using both HT and room temperature XRD, showing that U_3O_8 is metastable at 600 °C.

Conclusion

The thermal decomposition of ammonium diuranate in air up to 1000 °C was investigated, using in situ HT-XRD, TG/DTA. The results show that these two techniques are necessary and complementary to retrace the full process. Also in the framework of nuclear forensic investigations, XRD appears a useful technique for re-establishing the history of the heat treatment of uranium oxide of unknown origin. Such HT-XRD studies could be extended to other types of yellow cake material to complete the information basis on uranium oxide produced from different starting materials.

Acknowledgements We thank G. Pagliosa and D. Bouëxière for their technical support in the X-ray diffraction. H. Hein and M. Ernstberger are also acknowledged for help with the thermogravimetry/differential thermal analyses.

Open Access This article is distributed under the terms of the Creative Commons Attribution License which permits any use, distribution, and reproduction in any medium, provided the original author(s) and the source are credited.

References

- Mayer K, Wallenius M, Ray I (2005) Nuclear forensics: a methodology providing clues on the origin of illicitly trafficked nuclear materials. *Analyst* 130:433–441
- Wallenius M, Mayer K, Ray I (2006) Nuclear forensic investigations: two case studies. *Forensic Sci Int* 156(1):55–62
- Mayer K, Wallenius M, Fanghänel T (2007) Nuclear forensic science: from cradle to maturity. *J Alloy Compd* 444–445:50–56
- Wallenius M, Lützenkirchen K, Mayer K, Ray I et al (2007) Nuclear forensic investigations with a focus on plutonium. *J Alloy Compd* 444–445:57–62
- Badaut V, Wallenius M, Mayer K (2009) Anion analysis in uranium ore concentrates by ion chromatography. *J Radioanal Nucl Chem* 280(1):57–61
- Keegan E, Wallenius M, Mayer K, Varga Z, Rasmussen G (2012) Attribution of uranium ore concentrates using elemental and anionic data. *Appl Geochem* 27(8):1600–1609
- Cordfunke EHP (1970) Composition and structure of ammonium uranates. *J Inorg Nucl Chem* 32:3129–3131
- Cordfunke EHP (1962) On the uranates of ammonium-I. The ternary system $NH_3-UO_3-H_2O$. *J Inorg Nucl Chem* 24:303–307
- Debets PC, Loopstra BO (1963) On the uranates of ammonium-II X-ray investigation of the compounds in the system $NH_3-UO_3-H_2O$. *J Inorg Nucl Chem* 25:945–953
- Mea Hermans, Markestein T (1963) Ammonium uranates and UO_3 -hydrates-ammoniates. *J Inorg Nucl Chem* 25:461–462
- Stuart WI, Whateley TL (1969) Composition and structures of ammonium uranates. *J Inorg Nucl Chem* 31:1639–1647
- Stuart WI, Miller DJ (1973) The nature of ammonium uranates. *J Inorg Nucl Chem* 35(6):2109–2111
- Urbanek V, Sara V, Moravec J (1979) Study of formation and composition of ammonium uranates. *J Inorg Nucl Chem* 41:537–540
- Woolfrey JL (1978) The preparation of UO_2 powder: effect of ammonium uranate properties. *J Nucl Mater* 74:123–131
- Manna S, Roy SB, Joshi JB (2012) Study of crystallization and morphology of ammonium diuranate and uranium oxide. *J Nucl Mater* 424:94–100
- J.L.Woolfrey (1968) The preparation and calcination of ammonium uranates: A literature survey. Australian Atomic Energy Commission, AAEC/TM476
- Price GH, Stuart WI (1973) Thermal decomposition of ammonium uranates. Australian Atomic Energy Commission, AAEC/E276
- Manna S, Karthik P, Mukherjee A, Banerjee J, Roy SB, Joshi JB (2012) Study of calcinations of ammonium diuranate at different temperatures. *J Nucl Mater* 426:229–232
- Thein SM and Bereolos PJ (2000) Thermal Stabilization of $^{233}UO_2$, $^{233}UO_3$, $^{233}U_3O_8$. Oak Ridge National Laboratory, ORNL/TM-2000/82
- Litz JE and Coleman RB (1980) Production of yellow cake and uranium fluorides In: Advisory Group Meeting, Paris, 1979. International Atomic Energy Agency, Vienna, STI/PUB/553, ISBN 92-0-041080-4
- Ackermann RJ, Chang AT, Sorrell CA (1977) Thermal expansion and phase transformation of the U_3O_{8-z} phase in air. *J Inorg Nucl Chem* 39(1):75–85
- Hoekstra HR, Siegel S (1961) The uranium-oxygen system: $U_3O_8-UO_3$. *J Inorg Nucl Chem* 18:154–165
- Morss LR, Edelstein NM, Fuger J, Katz JJ (2006) The chemistry of the actinide and transactinide elements, vol 1, 3rd edn. Springer, Dordrecht
- Lynch ED (1965) Studies of stoichiometric and hyperstoichiometric solid solutions in the thoria-urania system. Argonne National Laboratory, ANL-6894
- Malinin GV, Tolmachev YM (1968) Differential thermal analysis of the decomposition of U_3O_8 in air. *Radiokhimiya* 10(3):362–366
- Herak R (1969) The crystal structure of the high temperature modification of U_3O_8 . *Acta Crystallogr B* 25:2505–2508
- Katz JJ, Seaborg GT, Morss LR (1986) The chemistry of the actinide elements, vol 1, 2nd edn. Chapman and Hall, New York
- Caneiro A, Abriata JP (1984) Equilibrium oxygen partial pressure and phase diagram of the uranium–oxygen system in the composition range $2.61 < U/O < 2.67$ between 844 and 1371 K. *J Nucl Mater* 126(3):255–267
- Loopstra B (1970) The structure of [beta]- U_3O_8 . *Acta Crystallogr Sect B* 26(5):656–657